Rapid thermal anneal activates light induced degradation due to copper redistribution

N. Nampalli,[1] H. S. Laine,[1] J. Colwell,[2] V. Vähänissi,[1] A. Inglese,[1] C. Modanese,[1] H. Vahlman,[1] M. Yli-Koski,[1] and H. Savin[1,a)]
[1]*Department of Electronics and Nanoengineering, Aalto University, Tietotie 3, Espoo 02150, Finland*
[2]*School of Photovoltaic and Renewable Energy Engineering, University of New South Wales, Sydney 2052, Australia*

(Received 13 March 2018; accepted 5 July 2018; published online 18 July 2018)

While it is well known that copper impurities can be relatively easily gettered from the silicon bulk to the phosphorus or boron–doped surface layers, it has remained unclear how thermally stable the gettering actually is. In this work, we show experimentally that a typical rapid thermal anneal (RTA, a few seconds at 800 °C) used commonly in the semiconductor and photovoltaic industries is sufficient to release a significant amount of Cu species from the phosphorus-doped layer to the wafer bulk. This is enough to activate the so-called copper-related light-induced degradation (Cu-LID) which results in significant minority carrier lifetime degradation. We also show that the occurrence of Cu-LID in the wafer bulk can be eliminated both by reducing the RTA peak temperature from 800 °C to 550 °C and by slowing the following cooling rate from 40–60 °C/s to 4 °C/min. The behavior is similar to what is reported for Light and Elevated Temperature degradation, indicating that the role of Cu cannot be ignored when studying other LID phenomena. Numeric simulations describing the phosphorus diffusion and the gettering process reproduce the experimental trends and elucidate the underlying physical mechanisms. https://doi.org/10.1063/1.5029347

Crystalline silicon is well known to suffer from so called carrier or light induced degradation (LID), which means that upon exposure to excess carriers, the bulk minority carrier lifetime can degrade significantly deteriorating the silicon device performance. The LID phenomenon has been a topic for a long debate, but even today, the exact defect reactions behind it remain ambiguous. However, at least one of the mechanisms seems to be well understood by now, that is, light interacting with benign positively charged interstitial copper (Cu) ions that form recombination-active nano-precipitates.[1] Such a phenomenon is currently referred to as copper-related light-induced degradation (Cu-LID). Further, Cu concentrations as low as $10^{10}\,\mathrm{cm}^{-3}$, which can easily be present in *p*-type commercial silicon or industrial processing lines,[2] have been shown to cause significant Cu-LID, especially in the presence of crystal defects.[3]

It is well established that, as a fast-diffusing transition metal, Cu can be relatively easily gettered to the n^+ or p^+ surface layer in an industrial device process.[4] Recent theoretical work[5,6] has speculated that rapid (<1 min), high temperature (peak at 800 °C) anneals after gettering can significantly increase the bulk metal point defect concentration and thus negate the gettering benefit for Cu and other fast-diffusing metals. However, this has not been shown experimentally, and moreover, the models used[7–9] have been validated based on steady-state experiments, which casts doubt on their validity under such rapid non-equilibrium processes. Thus, it is important to fill the critical gap in the literature by experimentally investigating how stable the gettering result is under these rapid, industry-typical anneals.

In this paper, we study experimentally (i) whether such a rapid thermal anneal (RTA) performed after a gettering step causes Cu to redistribute to the bulk and leads to the activation of Cu-LID and (ii) whether it is possible to modulate or even completely eliminate Cu-LID by modifying the RTA profile. The experiments are made with local Cu contaminated areas such that Cu-LID can be easily distinguished from other LID mechanisms. Supporting kinetic simulations to elucidate the physical root causes for our experimental observations are also performed. Finally, the implications of our findings for both the semiconductor and photovoltaic industries are discussed.

The experiments were performed on 380 ± 15 μm thick polished, boron-doped Cz-silicon wafers with a base doping density of $N_A \approx 4 \times 10^{15}\,\mathrm{cm}^{-3}$. The wafers were subjected to a one-sided phosphorus diffusion at 830 °C for 25 min in the $POCl_3$ gas atmosphere, which resulted in a phosphorus-doped layer with a sheet resistance of ∼80 Ω/□. During dopant diffusion, the rear side was protected with a 440 nm-thick thermal oxide, which also acted as a surface passivation layer, similar to the experiments described in Ref. 10. The thermal oxide was then thinned down to ∼20 nm by etching in a buffered HF solution, after which the central region of each wafer was then intentionally contaminated by depositing a droplet of copper sulphate solution (500 ppb w/v) on the rear side of the sample containing the thermal oxide (opposite to the phosphorus layer) in a well-defined area. The wafers were subsequently annealed at 800 °C for 20 min for Cu drive-in and then slowly cooled to 600 °C at a

a)Author to whom correspondence should be addressed: hele.savin@aalto.fi

controlled rate of 4 °C/min for efficient Cu gettering to the phosphorus-doped layer, similarly to that reported in Ref. 10. Localized contamination using a droplet allows for monitoring of the reference areas outside the contaminated region on the same wafer, which provides information about possible external contamination, e.g., during heat treatments. Likewise, the contribution of boron-oxygen or other LID defects can be directly observed from these areas and separated from Cu-LID.

Throughout the experiments, the wafers were characterized by minority-carrier lifetime using photoconductance measurements (Sinton Instruments WCT-120) in the generalized mode.[11,12] Surface photovoltage (Semilab WT-85X 400) and photoluminescence (PL) measurements (BT Imaging LIS-R1) were also performed.

To investigate the thermal redistribution of Cu, the wafers were then RTA treated in a Jipelec JetFirst RTP furnace in a nitrogen ambient. The wafers were placed on top of clean dummy wafers or a quartz boat, and the wafer temperatures were monitored with a thermocouple. The applied RTA time-temperature profiles with varying peak set-point temperatures (800 °C and 550 °C) and different cooling profiles (fast 40–60 °C/s, slow 4 °C/min) are presented in Fig. 1. Note that the 800F recipe is typical of screen printing RTA profiles carried out after emitter formation in industrial silicon solar cell processing.[13] Finally, after RTA, the wafers were immediately light-soaked to get an estimate of the Cu concentration redistributed to the bulk. Light soaking was performed for up to ~72 h with an LED light source having an intensity of 0.02 suns and a spectral range of 400–800 nm (maximum at 550 nm) with substrate temperature monitored and maintained at 27 ± 3 °C.

Figure 2 shows the PL images of the samples both before RTA treatments and after three different RTA treatments followed by light soaking. To confirm that the PL maps reflect changes only in the wafer bulk, the same samples were also measured by SPV (not shown), which is only sensitive to bulk lifetime. Both methods provided similar information, but only PL maps are shown here due to improved spatial resolution over SPV maps.

Based on the gettering experiments carried out earlier[10] and PL images shown in Fig. 2 (the first row), we confirmed that prior to RTA treatment, Cu was gettered to the phosphorus layer in all samples. On the contrary, when the same wafers were exposed to an RTA treatment at 800 °C with fast ramp-

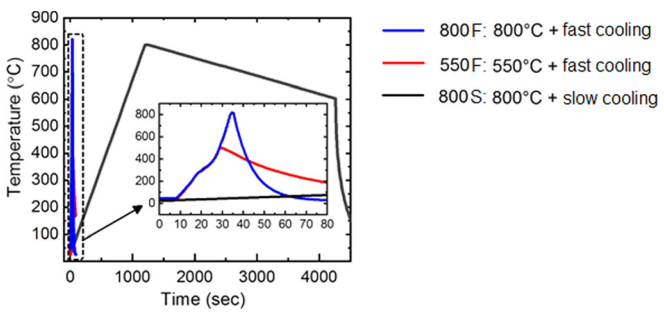

FIG. 1. RTA recipes with varying peak temperatures and different cooling profiles. Slow cooling was used in recipe 800S (black line) in the 800 °C to 600 °C range. The inset shows the details of the thermal profiles for the recipes 800F (blue line, 800 °C fast cool) and 550F (red line, 550 °C fast cool).

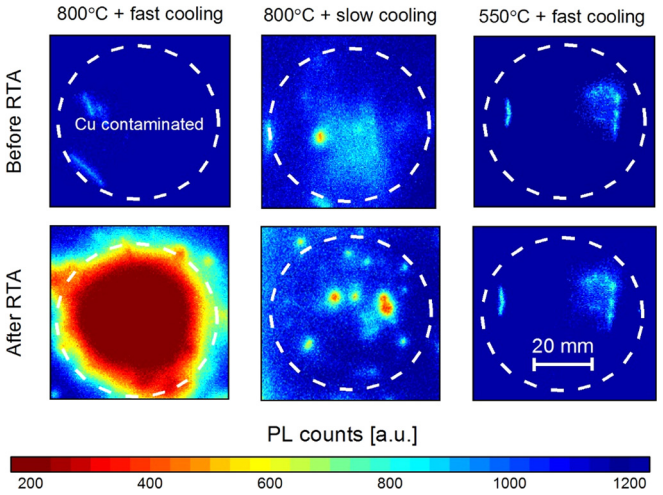

FIG. 2. PL images of the various samples in the Cu-contaminated regions. The top row presents PL maps after phosphorus diffusion and Cu contamination but before they were annealed in the RTA furnace. The bottom row shows PL images of the same wafers and areas after RTA and light soaking. The white dotted circles represent the areas which were intentionally copper contaminated with a Cu-droplet.

down (recipe 800F), a clear Cu-LID spot appeared in the PL map after light soaking (lower left map in Fig. 2). This result suggests that even a short rapid thermal anneal at 800 °C, which is typical for solar cell metal contact firing, is enough to thermally redistribute the gettered copper back to the wafer bulk. The PL images also show that in the reference areas (outside the Cu spot), no noticeable degradation takes place.

Further, PL images for recipe 550F after RTA and light soaking (lower right map in Fig. 2) display an interesting phenomenon: by reducing the RTA peak temperature to 550 °C, Cu-LID appears to be completely eliminated. This demonstrates that the peak RTA temperature has a clear impact on the amount of copper that is redistributed to the bulk and thus also on the appearance of Cu-LID. Thereby, it is likely that at $T_{peak} = 550$ °C, the amount of emerged Cu is greatly reduced in the bulk and is not high enough to activate Cu-LID.

In addition to peak temperature, the cooling rate of the RTA treatment also appears to impact Cu-LID (lower middle map in Fig. 2). With a peak temperature of 800 °C followed by slow cooling (recipe 800S), no sign of Cu-LID could be observed in the bulk of the wafer. Thus, it seems that the proper tuning of both the RTA peak temperatures and the subsequent cooling rates provides an effective way to eliminate or at least minimize Cu-LID.

To achieve more quantitative information about Cu-LID and to observe the kinetics of degradation, effective minority carrier lifetime (τ_{eff}) was measured as a function of light soaking time for all samples. The normalized defect density (N_t) associated with the LID effect was then calculated from the measured lifetime using Eq. (1) and is plotted in Fig. 3. Note that τ_{eff} was determined at a minority carrier density $\Delta n = 0.1 \times N_A$ (4×10^{15} cm^{-3}) for the purpose of calculating N_t

$$N_t(t) = \frac{1}{\tau_{eff}(t)} - \frac{1}{\tau_{eff}(t=0)}. \quad (1)$$

It can be seen from Fig. 3 that, as expected, the sample with the most prominent Cu-contamination spot (800F,

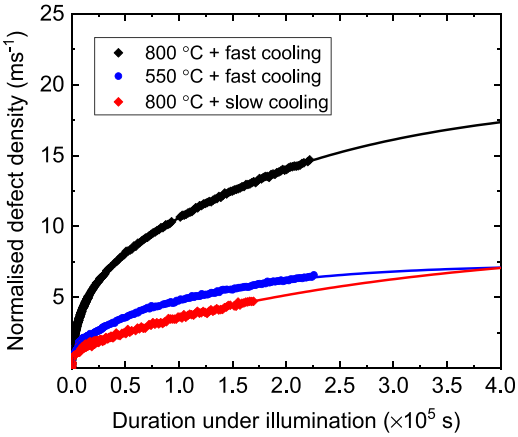

FIG. 3. Temporal evolution of normalized defect density (N_t) showing the extent and kinetics of LID in samples treated with Recipes 800F (black), 800S (red), and 550F (blue). Lines represent exponential fits to $N_t(t)$.

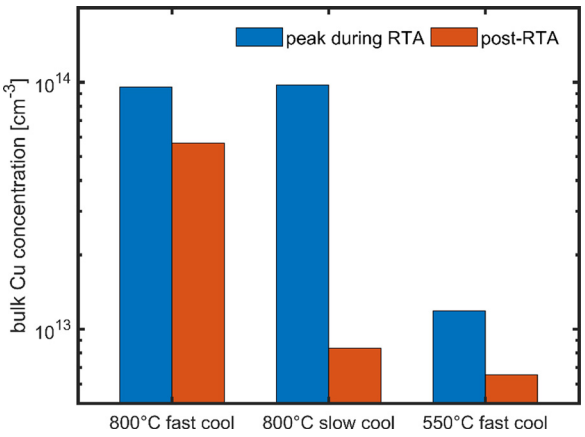

FIG. 4. Simulated peak bulk Cu concentration (blue bars) during the RTA treatments as well as the post-RTA bulk Cu concentration (red bars) for different RTA profiles.

bottom left in Fig. 2) also demonstrates the fastest degradation kinetics as well as the maximum extent of degradation (black curve in Fig. 3). As an indicative value, the normalized defect density after 1 h of degradation (3600 s) was 2.58 ms^{-1} for the 800F sample, whereas samples 800S and 550F showed significantly lower N_t values of 1.14 ms^{-1} (~55% less) and 1.51 ms^{-1} (~41% less), respectively. The slight degradation in the 800S and 550F samples in Fig. 3 was confirmed to be primarily due to the BO-defect based on its known degradation kinetics, *i.e.,* following the procedure described in Ref. 1.

To further elucidate the physical root causes of the experimental observations, the behavior of Cu during the different RTA treatments was simulated. This was done by modelling the re-distribution of Cu in one dimension along the wafer depth due to segregation into the heavily phosphorus-doped layer, using the quantitative segregation model presented and validated in Ref. 14. No internal gettering sources, such as structural defects or oxygen precipitates, were assumed in the simulation. Within the boron-doped bulk, the solubility of Cu was calculated as in Eq. (15) in Ref. 15 and the diffusivity as in Ref. 16. Within the heavily phosphorus-doped layer, the diffusivity of Cu was assumed to be $D_{eff} = \frac{D_{int}}{k_{S,Cu}}$, where $k_{S,Cu}$ is the ratio of Cu solid solubility in the emitter and bulk (segregation coefficient) as calculated from Ref. 14.

The phosphorus diffusion process was simulated as suggested by Ref. 9, assuming a surface phosphorus concentration of 3×10^{20} cm^{-3}.[17] The only varied input between the samples was the different thermal profiles of the RTA process. Other inputs that were held constant for all samples included wafer thickness, boron base doping concentration, and the thermal profiles of the $POCl_3$ diffusion and copper in-diffusion processes.

Figure 4 shows the simulated evolution of the bulk Cu concentration during the three experimental RTA treatments, with concentrations at peak sample temperature during RTA and after RTA shown separately. There are 2 important observations here. First, it can be seen that the Cu concentration in the bulk at the peak of the RTA process (blue bar in Fig. 4) is higher by an order of magnitude for the 800F and 800S recipes compared to the 550F recipe and is roughly equal for both the 800F and 800S recipes. This result is expected since the Cu solubility difference between the bulk and the emitter is approximately three orders of magnitude higher at 550 °C than 800 °C (Fig. S1 bottom row, black dashed line), and thus, Cu prefers to stay in the emitter in the recipe 550F.

Second, it can be seen that after the RTA process is complete (i.e., after complete ramp-down, red bar in Fig. 4), all three samples display a lower Cu concentration in the bulk compared to just before the ramp-down (blue bar). However, the degree to which this occurs is different for the three samples. In general, the bulk Cu concentration decreases during ramp-down by an order of magnitude in the slow-cooled sample (800S), but to a lesser degree in the fast-cooled samples (800F, 550F). This can be understood due to the (more strongly) kinetically limited nature of the 550F and 800F recipes. It can be seen that during the slow cool-down of the 800S sample, the actual Cu concentration difference between the emitter and the bulk follows closely that of the solubility difference (solid and dashed black lines, Fig. S1(i), which is not the case for the fast cooled samples [Figs. S1(g)–S1(h)]. Furthermore, the Cu diffusivity remains high for a much longer time in the recipe 800S (red line, Fig. S1 bottom row), which allows more Cu to segregate back to the emitter especially during the final cooling and, on the other hand, explains why in the fast-cooled samples (800F and 550F), the post-RTA bulk Cu concentration is only 30%–40% lower compared to the value at the process peak temperature. The kinetics of Cu redistribution during the RTA treatments are described in further detail in the supplementary material, and the impact of the anneals on solar cell parameters is modelled further in Ref. 18.

Note that the total Cu concentration present in the samples could not be directly measured, and therefore, the absolute Cu concentrations from the simulations may not correspond directly to those present in the samples. The specific simulated total Cu concentration was 10^{14} cm^{-3}. Nevertheless, simulated trends between the three cooling profiles persist with varying simulated total Cu concentrations. For example, a factor of two higher total Cu concentration results in exactly a factor of two higher bulk final Cu concentrations in all samples.

Indeed, the trends from the simulations are consistent with the experimental observations in Figs. 2 and 3, with the 800 °C fast-cool RTA leading to the most severe Cu-LID as

well as displaying significantly higher post-RTA bulk Cu concentration in the simulations compared to the other two samples. Thus, the simulations offer a plausible physical root cause for the observed experimental behavior.

To summarize, the experimental and simulation results in this study demonstrate that RTA can cause significant thermal redistribution of Cu point defects from the phosphorus-doped layer back to the wafer bulk. For the semiconductor industry, the results give insights into the thermal stability of Cu gettering in the device fabrication. Although this study focused on copper, the thermal stability of gettering of other fast diffusing metal impurities, such as nickel, cobalt, and iron, can be questioned as well. For example, it has been reported that RTA can dissolve iron precipitates in the bulk[19,20] while this study implies that the measured increased interstitial iron concentration could also be due to iron diffusion from the phosphorus layer. On the other hand, there are also opposite results showing that the presence of a phosphorous emitter during subsequent anneals increases the minority carrier lifetime.[21] So far, iron redistribution from the phosphorus layer has been verified only with very long anneals (1 h).[22,23] Finally, while this study focuses on Cu gettering by phosphorus emitters, it is plausible that a similar redistribution could also occur after RTA if Cu is gettered by aluminum back-surface fields (Al-BSF),[24] boron-rich layers,[25] or dielectric films.[26]

For the photovoltaic industry, these results highlight the fact that the final processing step for silicon solar cell fabrication, namely, RTA of screen printed metal contacts, can be the origin of severe Cu-LID. Further, this study also demonstrates a clear potential for mitigating Cu-LID via the use of slower cooling rates after high temperature anneals and/or lower peak temperatures. Finally, the observations in this study are also particularly significant for investigations into other LID effects such as the so called Light and elevated Temperature Induced Degradation (LeTID) and boron-oxygen LID (BO-LID). These LID mechanisms are also known to be modulated during RTA and/or activated by RTA.

In particular, Eberle *et al.*[27,28] observed that a fast ramp rate in RTA induces strong LeTID, while a slower ramp rate practically eliminates it—which is similar to the behaviour observed in this study. Furthermore, several other studies[29–32] have consistently reported that the magnitude of LeTID increases with peak firing temperature, with peak temperatures $\leq$650 °C leading to little or no LeTID, while temperatures between 700 °C and 950 °C trigger degradation. These trends in degradation behaviour with firing temperature and cooling rate correlate well with the present study. In contrast to LeTID, an increase in peak firing temperature and cooling rate is known to decrease the magnitude of BO-LID,[33,34] which is opposite to the trend observed here. However, an increase in non-BO related LID has been observed in Cz silicon at peak firing temperatures above ~650 °C.[33,35] While such effects have been attributed to LeTID,[36,37] the possibility of Cu-LID being responsible for such LID effects has not been specifically precluded in such studies. It must be noted that there exist other empirical differences between LeTID and Cu-LID (*e.g.,* SRH properties[29,38,39] and activation energy of degradation[31,38]). However, Cu concentrations as low as 10^{10} cm^{-3} have been shown to induce Cu-LID,[40] although the threshold concentration depends on the substrate quality. Therefore, it can be concluded that if copper exists in sufficiently high concentrations in wafers used in the investigation of these other LID effects (particularly LeTID), it is likely that the observed degradation effects in such cases can be at least partially attributed to Cu-LID.

See supplementary material for the full time-dependent simulations of segregation coefficient, diffusivity, and copper distribution during the rapid thermal anneals studied in this paper.

The authors from Aalto University acknowledge funding from the European Research Council under the European Union's FP7 Programme ERC Grant Agreement No. 307315. H.L. also acknowledges Finnish Cultural Foundation, and J.C. acknowledges the receipt of a Research Training Program (RTP) Scholarship from the Australian Government. The views expressed herein are not necessarily the views of the Australian Government, and the Australian Government does not accept responsibility for any information or advice contained herein.

[1]H. Vahlman, A. Haarahiltunen, W. Kwapil, J. Schön, A. Inglese, and H. Savin, J. Appl. Phys. **121**(19), 195704 (2017).
[2]G. Coletti, Prog. Photovoltaics Res. Appl. **21**, 1163–1170 (2013).
[3]H. Väinölä, E. Saarnilehto, M. Yli-Koski, A. Haarahiltunen, J. Sinkkonen, G. Berenyi, and T. Pavelka, Appl. Phys. Lett. **87**(3), 32109 (2005).
[4]M. B. Shabani, T. Yamashita, and E. Morita, ECS Trans. **16**, 179–193 (2008).
[5]M. A. Jensen, A. E. Morishige, S. Chakraborty, R. Sharma, H. S. Laine, B. Lai, V. Rose, A. Youssef, E. E. Looney, S. Wieghold *et al.*, IEEE J. Photovoltaics **8**(2), 448–455 (2018).
[6]A. E. Morishige, H. S. Laine, J. Schön, A. Haarahiltunen, J. Hofstetter, C. del Cañizo, M. C. Schubert, H. Savin, and T. Buonassisi, Appl. Phys. A **120**(4), 1357–1373 (2015).
[7]A. Haarahiltunen, H. Väinölä, O. Anttila, M. Yli-Koski, and J. Sinkkonen, J. Appl. Phys. **101**(4), 43507 (2007).
[8]A. Haarahiltunen, H. Savin, M. Yli-Koski, H. Talvitie, and J. Sinkkonen, J. Appl. Phys. **105**(2), 23510 (2009).
[9]A. Bentzen, A. Holt, J. S. Christensen, and B. G. Svensson, J. Appl. Phys. **99**(6), 64502 (2006).
[10]A. Inglese, H. S. Laine, V. Vähänissi, and H. Savin, AIP Adv. **8**(1), 15112 (2018).
[11]H. Nagel, C. Berge, and A. G. Aberle, J. Appl. Phys. **86**(11), 6218 (1999).
[12]A. Richter, S. W. Glunz, F. Werner, J. Schmidt, and A. Cuevas, Phys. Rev. B **86**(16), 165202 (2012).
[13]*Dupont Solamet PV19A Screen Print Paste-Preliminary Data Sheet* (DuPont Microcircuit Materials, 2015).
[14]R. Hoelzl, K.-J. Range, and L. Fabry, Appl. Phys. A: Mater. Sci. Process. **75**(4), 525–534 (2002).
[15]H. Vahlman, A. Haarahiltunen, W. Kwapil, J. Schön, A. Inglese, and H. Savin, J. Appl. Phys. **121**(19), 195703 (2017).
[16]A. A. Istratov, C. Flink, H. Hieslmair, E. R. Weber, and T. Heiser, Phys. Rev. Lett. **81**(6), 1243–1246 (1998).
[17]J. Hofstetter, D. P. Fenning, M. I. Bertoni, J. F. Lelièvre, C. del Cañizo, and T. Buonassisi, Prog. Photovoltaics Res. Appl. **19**(4), 487–497 (2011).
[18]H. S. Laine, H. Vahlman, A. Haarahiltunen, M. A. Jensen, C. Modanese, M. Wagner, F. Wolny, T. Buonassisi, and H. Savin, in 8th International Conference on Crystalline Silicon Phovoltaics, 2018.
[19]J. Schön, M. C. Schubert, H. Habenicht, and W. Warta, in *Proceedimgs 25th European Photovoltaic Solar Energy Conference* (2010), pp. 1195–1199.
[20]J. F. Lelièvre, J. Hofstetter, A. Peral, I. Hoces, F. Recart, and C. Del Cañizo, Energy Proc. **8**, 257–262 (2011).
[21]J. Tan, D. Macdonald, N. Bennett, D. Kong, A. Cuevas, and I. Romijn, Appl. Phys. Lett. **91**(4), 43505 (2007).

[22]D. Macdonald, A. Cheung, and A. Cuevas, in *Proceedings of the 3rd World Conference on Photovoltaic Energy Conversion* (2003), pp. 1336–1339.
[23]A. Haarahiltunen, M. Yli-Koski, and H. Savin, Energy Proc. **8**, 355–359 (2011).
[24]P. S. Plekhanov, M. D. Negoita, and T. Y. Tan, J. Appl. Phys. **90**(10), 5388–5394 (2001).
[25]S. P. Phang, W. Liang, B. Wolpensinger, M. A. Kessler, and D. Macdonald, IEEE J. Photovoltaics **3**(1), 261–266 (2013).
[26]A. Y. Liu, C. Sun, V. P. Markevich, A. R. Peaker, J. D. Murphy, and D. Macdonald, J. Appl. Phys. **120**(19), 193103 (2016).
[27]R. Eberle, W. Kwapil, F. Schindler, M. C. Schubert, and S. W. Glunz, Phys. Status Solidi-Rapid Res. Lett. **10**(12), 861–865 (2016).
[28]R. Eberle, W. Kwapil, F. Schindler, S. W. Glunz, and M. C. Schubert, Energy Proc. **124**, 712–717 (2017).
[29]K. Nakayashiki, J. Hofstetter, A. E. Morishige, T. A. Li, D. B. Needleman, M. A. Jensen, and T. Buonassisi, IEEE J. Photovoltaics **6**(4), 860–868 (2016).
[30]C. E. Chan, D. N. R. Payne, B. J. Hallam, M. D. Abbott, T. H. Fung, A. M. Wenham, B. S. Tjahjono, and S. R. Wenham, IEEE J. Photovoltaics **6**(6), 1473–1479 (2016).
[31]D. Bredemeier, D. Walter, S. Herlufsen, and J. Schmidt, Energy Proc. **92**, 773–778 (2016).
[32]C. Vargas, K. Kim, G. Coletti, D. Payne, C. Chan, S. Wenham, and Z. Hameiri, IEEE J. Photovoltaics **8**(2), 413–420 (2018).
[33]N. Nampalli, H. Li, M. Kim, B. Stefani, S. Wenham, B. Hallam, and M. Abbott, Sol. Energy Mater. Sol. Cells **173**, 12–17 (2017).
[34]D. C. Walter, B. Lim, K. Bothe, V. V. Voronkov, R. Falster, and J. Schmidt, Appl. Phys. Lett. **104**(4), 42111 (2014).
[35]N. Nampalli, "Characterisation and passivation of boron-oxygen defects in p-type Czochralski silicon," Ph.D. thesis, University of New South Wales, Australia, 2017.
[36]D. Chen, M. Kim, B. V. Stefani, B. J. Hallam, M. D. Abbott, C. E. Chan, R. Chen, D. N. R. Payne, N. Nampalli, A. Ciesla *et al.*, Sol. Energy Mater. Sol. Cells **172**, 293–300 (2017).
[37]D. Chen, P. G. Hamer, M. Kim, G. Bourret-Sicotte, S. Liu, A. Ciesla, C. E. Chan, R. Chen, T. H. Fung, C. Vargas *et al.*, in 8th International Conference on Crystalline Silicon Phovoltaics, 2018.
[38]J. Lindroos and H. Savin, Sol. Energy Mater. Sol. Cells **147**, 115–126 (2016).
[39]C. Vargas, Y. Zhu, G. Coletti, C. Chan, D. Payne, M. Jensen, and Z. Hameiri, Appl. Phys. Lett. **110**(9), 92106 (2017).
[40]H. Väinölä, E. Saarnilehto, M. Yli-Koski, A. Haarahiltunen, and J. Sinkkonen, Appl. Phys. Lett. **87**(3), 032109 (2005).